Neural dysfunction at the upper thermal limit in the zebrafish

Anna H. Andreassen[*] & Petter Hall[*], Pouya Khatibzadeh, Fredrik Jutfelt, Florence Kermen[#]

[*] These authors contributed equally.

[#] Corresponding author: florence.kermen@ntnu.no

Authors affiliation

Department of Biology, Faculty of Natural Sciences, Norwegian University of Science and Technology, 7491 Trondheim, Norway.

Keywords: heat stress, spreading depolarization, CT_{max}, thermal tolerance, central nervous system, calcium imaging, zebrafish

Highlights

- Larval zebrafish reach their critical thermal limit (CT_{max}) at similar temperature as adult zebrafish
- Acute heat stress causes a brain-wide spreading depolarization near the upper thermal limit
- CT_{max} precedes brain-wide depolarization
- Heart rate declines at high temperatures but is maintained during CT_{max} and brain depolarization
- Neural activity is impaired prior to CT_{max} and brain-wide depolarization
- Oxygen availability in the water affects both CT_{max} and neural activity

ABSTRACT

Understanding animal thermal tolerance is crucial to predict how animals will respond to increasingly warmer temperatures, and to mitigate the impact of the climate change on species survival. Yet, the physiological mechanisms underlying animal thermal tolerance are largely unknown. In this study, we developed a method for measuring upper thermal limit (CT_{max}) in larval zebrafish (*Danio rerio*) and found that it occurs at similar temperatures as in adult zebrafish. We discovered that CT_{max} precedes a transient, heat-induced brain-wide depolarization during heat ramping. By monitoring heart rate, we established that cardiac function is sub-optimal during the period where CT_{max} and brain depolarization occur. In

addition, we found that oxygen availability affects both locomotor neural activity and CT_{max} during a heat stress. The findings of this study suggest that neural impairment due to limited oxygen availability at high temperatures can cause CT_{max} in zebrafish.

INTRODUCTION

Periods of abnormally high temperatures are becoming more numerous and severe as climate change progresses (Seneviratne *et al.*, 2014; Stillman, 2019). As biological rates are highly affected by temperature, animals that hold similar body temperatures as the surrounding environment (i.e. ectotherms) might be particularly vulnerable to extreme heat (Deutsch *et al.*, 2008; Schulte, 2015; Pinsky *et al.*, 2019). Under acute heating, ectotherms reach a critical thermal limit (CT_{max}), a temperature where their equilibrium is lost and their movement becomes disorganized (Friedlander *et al.*, 1976; Morgan *et al.*, 2018; Jørgensen *et al.*, 2020). The thermal tolerance of ectotherms correlates with their geographical distributions (Perry *et al.*, 2005; Sunday *et al.*, 2012), suggesting that limits in thermal tolerance partly determines distribution ranges. Moreover, rapid onset of heat waves can cause mass mortality in fishes, which suggests that thermal tolerance can be an increasingly important trait in the future (Genin *et al.*, 2020).

Knowledge about the mechanisms controlling thermal tolerance is therefore important to understand how ectotherms may respond to increasingly warmer temperatures and predict ecosystem impacts. Although the physiological mechanisms of thermal tolerance are largely unknown, two major bottlenecks have been proposed; oxygen limitation and neural dysfunction (Friedlander *et al.*, 1976; Pörtner *et al.*, 2017; Jutfelt *et al.*, 2019).

The oxygen limitation view (i.e. the oxygen- and capacity-limited thermal tolerance (OCLTT) hypothesis) suggests that tissue oxygen shortage limits thermal tolerance under acute heat stress (Pörtner & Knust, 2007; Ern, 2019). According to this hypothesis, the cardiorespiratory system in ectotherms is unable to match the increasing oxygen requirement with temperature, leading to tissue hypoxia and thus setting the limits for thermal tolerance. Insufficient cardiorespiratory function at high temperature, or near upper thermal limit, has been reported in insects and fish (Pörtner, 2002; Farrell, 2007, 2009; Ern *et al.*, 2014), but it is maintained in a number of other ectotherms (Ern *et al.*, 2015). In addition, experimental manipulation of oxygen availability during heat stress does not always affect thermal tolerance (McArley *et al.*, 2020). These contrasting results suggest that oxygen limitation can only partly explain thermal

tolerance, which is likely limited by different mechanisms in various species and contexts (Ern *et al.*, 2016; Lefevre, 2016; Verberk *et al.*, 2016; Jutfelt *et al.*, 2018, 2019). Furthermore, the OCLTT hypothesis does not specify which physiological mechanisms fail first due to tissue hypoxia (Jutfelt *et al.*, 2018).

Efficient locomotion (which is impaired at CT_{max}) requires normal neural function that is disrupted at high temperature. Therefore, neural control of locomotion is a heat-sensitive physiological mechanism that could underlie upper thermal tolerance, either via direct thermal effects on neurons (Friedlander *et al.*, 1976; Jutfelt *et al.*, 2019) or via indirect thermal effects from oxygen limitations (Schulte, 2015). Examples of severe heat-induced neural dysfunctions include spreading depolarizations in fruit fly (Jørgensen *et al.*, 2020), loss of rhythmic neural activity in the digestive system of the crab (Marder *et al.*, 2015), and thermogenic seizures in vertebrates (Dube *et al.*, 2000; Shinnar & Glauser, 2002; Hunt *et al.*, 2012). Yet, very few studies have directly investigated how neural dysfunction relates to measures of thermal tolerance. In the fruit fly, spreading depolarizations measured in head-restrained flies occur at similar temperatures as heat-induced coma in freely moving conspecifics (Jørgensen *et al.*, 2020). Similarly, goldfish lose equilibrium at temperatures that induce hyperexcitability in cerebellar neurons of anesthetized conspecifics (Friedlander *et al.*, 1976), and a study on Atlantic cod (*Gadus morhua*) found that cooling the brain marginally increased CT_{max}, suggesting a causal link between brain function and thermal tolerance (Jutfelt *et al.*, 2019).

The relative importance of cardiorespiratory and oxygen limitations, versus direct thermal impacts on neuronal function, as the mechanisms limiting thermal tolerance during warming remains unclear (Clark *et al.*, 2013a, 2013b; Jutfelt *et al.*, 2014, 2018, 2019). This is partly due to the challenge of recording brain activity and CT_{max} in the same freely moving animal. In this study, we solved that challenge by simultaneously measuring brain activity and locomotion during heating using non-invasive fluorescence imaging in transparent larval zebrafish (*Danio rerio*) expressing a calcium indicator in the brain. We also recorded heart rate simultaneously with neural activity during heating in a separate group of larval zebrafish. Finally, we measured CT_{max} and neural activity in hypo- and hyperoxic conditions. This allowed us to test two predictions. First, if dysfunction of the central nervous system limits thermal tolerance, neural dysfunction should briefly precede or coincide with CT_{max}. Second, if neural dysfunction is caused by a cardiorespiratory limitation, we predict that failure of cardiac function precedes neural malfunction, and that water oxygen manipulation affects neural function and CT_{max}.

RESULTS

CT_{max} is similar in larval and adult zebrafish

The activity and upper thermal limit (CT_{max}) were recorded in freely swimming five-day-old larval zebrafish in a custom-designed glass chamber (**Figure 1A**, **B**), in which water temperature increased from 28°C at a rate of 0.3°C/min (heat ramp fish), or was maintained at 28°C (control fish). To measure the activity level of larval zebrafish in our set-up, we recorded swimming speed (**Figure S1**), episodes of disorganized swimming (spiral swimming, **Movie S1**) and loss of equilibrium (**Movie S2**) at selected temperature ranges during the heat ramp. The swimming speed of five-day-old zebrafish decreased on average from 2.9±0.6 mm/s to 1.7±0.3 mm/s during the assay, at a similar rate in the control and the heat ramp fish (linear mixed-effects model, time: β±S.E.=0.3±0.1, $t_{(103)}$=-2.5, p=0.013; treatment: β±S.E.=0.8±0.6, $t_{(24)}$=1.2, p=0.23, R^2=0.1, **Figure S1**). Ten of the 12 heat ramp fish, but none of the 14 control fish, displayed episodes of disorganized circular swimming prior to CT_{max} (Chi-square: $X^2_{(df=1,N=26)}$=15.6, p<0.001; **Figure 1C**). Animals close to their upper thermal limit often lose equilibrium, a behavioural event that is commonly used to determine CT_{max} across species (Moyano *et al.*, 2017; Morgan *et al.*, 2018). Here, we found that the heat ramp fish were unable to maintain equilibrium 15.3% of the time, more frequently than control fish, which lost equilibrium 0.8% of the time (Wilcoxon rank sum test, heat ramp: median±IQR=15.3±13.7%, control: 0.8±6.8%, r=0.58, p=0.004, **Figure 1D**). Yet, half of the control fish lost equilibrium during the assay (**Figure 1D**), likely because five-day-old zebrafish do not completely master postural stability.

We therefore measured CT_{max} as the temperature at which zebrafish larvae repeatedly failed to escape touches to the trunk (loss of response, see **Methods**). Using this loss of response criterion, five-day-old heat ramp fish reached CT_{max} at 41.4±0.1°C (**Figure 1E**). Nine-day-old fish tested in the same setup reached CT_{max} at similar temperatures of 41.3±0.2°C, indicating that the loss of response criterium is stable during larval development (linear regression model, nine-day-old: β±S.E.=-0.1±0.2°C, $t_{(36)}$=-0.5, p=0.7, **Figure 1E**). Furthermore, adults from the same line tested using the loss of equilibrium protocol (Morgan *et al.*, 2018), reached CT_{max} at similar temperatures (41.0±0.1°C) as larvae (adult: β±S.E.=-0.4±0.2, $t_{(36)}$=-1.9, p=0.07; $F_{(2,36)}$=1.9, R^2=0.1, **Figure 1E**).

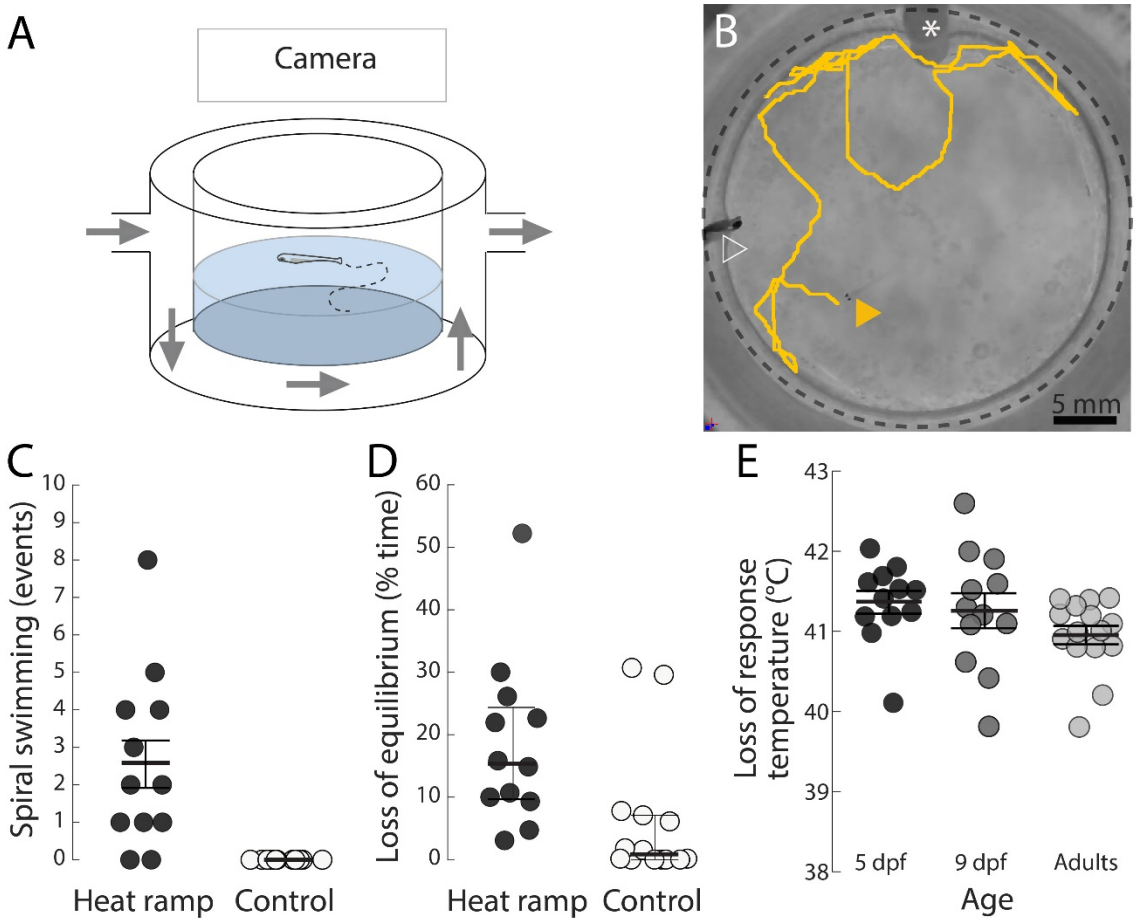

Figure 1. Disorganized locomotion and loss of response at upper thermal limit in freely swimming zebrafish larvae.
Schematic figure (**A**) and photo with top view (**B**) of the experimental setup for CT_{max} measurement in freely swimming zebrafish larva. **B.** Larva initial position is indicated by an orange, filled arrowhead. The larva's trajectory is represented in orange during the following 30 seconds. The dashed black circle indicates the walls of the central chamber. The white arrowhead indicates the position of a thermocouple. The white asterisk indicates the tube for bubbling. **C.** Number of spiral swimming events (see **Methods** and **Movie S1**) recorded during the 12 minutes preceding CT_{max} for five-day-old heat ramp fish (black circles, n=14), or during the corresponding period in the control fish (empty circles, n=12; Chi-squared test: $X^2_{(df=1,N=26)}=15.6$, $p<0.001$). **D.** Loss of equilibrium (% time, see **Methods** and **Movie S2**) in heat ramp and control fish during the same period as in **C** (Wilcoxon Rank Sum test: $r=0.58$, $p=0.004$). **E.** CT_{max} (loss of response, see **Methods**) temperature in five-day-old (n=12, black circles), nine-day-old (n=12, dark grey circles) and adult heat ramp fish (n=15, light grey circles; linear regression model, nine-day-old: β±S.E.=-0.1±0.2°C, $t_{(36)}=-0.5$, $p=0.7$; adult: β±S.E.=-0.4±0.2°C, $t_{(36)}=-1.9$, $p=0.07$; $F_{(2,36)}=1.9$, $R^2=0.1$; **Table S2**). The bars and error bars indicate the group mean and S.E. in **C** and **E**, and median and inter quartile range in **D**.

Warming causes a transient brain-wide depolarization near the upper thermal limit

Neurons operate best within a certain thermal range (Robertson & Money, 2012; Tang *et al.*, 2012; Marder *et al.*, 2015). Therefore, we hypothesized that a neural malfunction would occur as the fish's temperature approaches the upper thermal limit. To record neural activity in the entire zebrafish brain during a heat ramp, zebrafish larvae, expressing the calcium indicator GCaMP6s in all neurons, were mounted in agarose under an epifluorescence microscope

(**Figure 2A**, **B**). Calcium events were detected in the brainstem of heat ramp and control fish (**Figure 2C**, **D**). The frequency of the brainstem calcium events remained stable over time in the control fish (**Figure 2F**). In heat ramp fish, the frequency of brainstem calcium events increased with temperature, before abruptly declining (**Figure 2F**) during the 15 minute-period preceding a transient brain-wide depolarization (**Figure 2D**). The telencephalon and the brainstem, which are normally weakly co-active, both displayed a sharp increase in activity during the depolarization (**Figure 2D**). The brain-wide spread of the depolarization is further illustrated in laterally mounted fish (**Figure 2E**, **Movie S3**): it spread relatively slowly, and reached the dorsal brain regions 10-12 seconds after the onset in the ventral diencephalon (**Figure 2E**). The heat-induced brain-wide depolarizations started on average at 40.5±0.4°C in agar-embedded fish (**Figure 2G**), 0.8°C below the average CT_{max} temperature recorded in freely swimming age-matched fish (41.4±0.1°C, **Figure 1E**). Our results show that a transient brain-wide depolarization occurs during the heat ramp at temperatures close to CT_{max} in zebrafish.

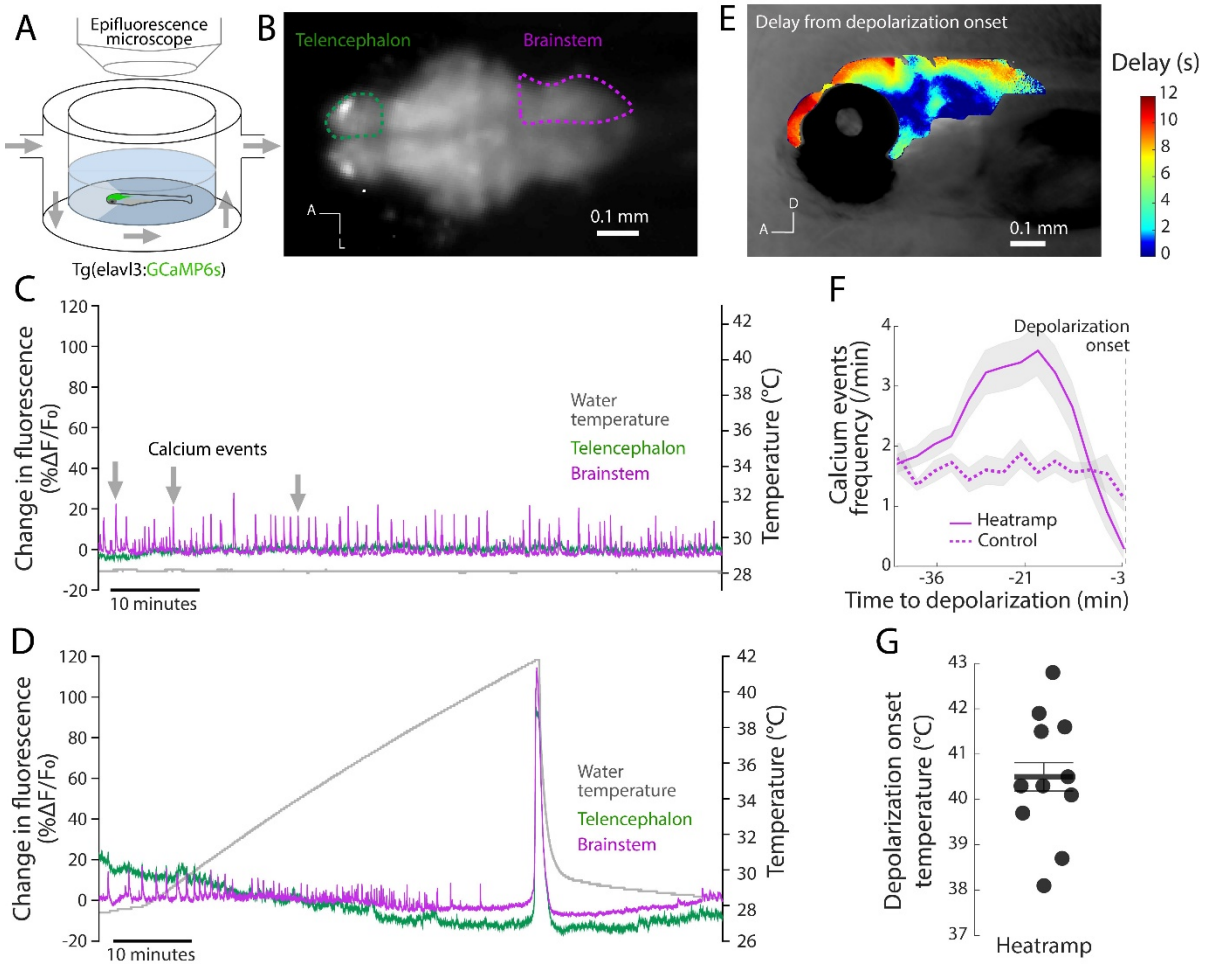

Figure 2. Embedded zebrafish larvae develop brain-wide depolarizations near the upper thermal limit. Schematic overview (**A**) and image (**B**) from the experimental setup for whole brain neural activity measurement

in agar-embedded five-day-old *Tg(elavl3:GCaMP6s)* zebrafish larva. **B.** Raw fluorescence image of the larva brain highlighting the right telencephalon (dashed green line) and brainstem (dashed magenta line; A=anterior, L=lateral). **C**, **D** Change in fluorescence (% $\Delta F/F_0$, left y-axis) in the telencephalon and brainstem of a representative control larva (**C**) and a representative heat ramp larva (**D**). The water temperature (grey) was maintained at 28°C throughout the recording (right y-axis, **C**) for the control fish and was increased during a heat ramp treatment (0.3°C/min) until a brain-wide depolarization was detected, and then rapidly adjusted to 28°C until the end of the recording (right y-axis, **D**). **E.** Heatmap illustrating the temporal spread of the depolarization throughout the brain in a representative heat ramp fish mounted laterally (see **Methods**; A=anterior, D=dorsal). **F.** Frequency of brainstem calcium events in heat ramp fish (n=11; magenta line) during the 50 minutes preceding the brain-wide depolarization, and during the corresponding period in control fish (n=8, magenta dashed line). The depolarization onset in heatramp fish is indicated by a dashed vertical line. **G.** Temperature at depolarization onset in heat ramp fish (40.5°C ±0.4, n=11). Data are presented with mean (solid line) and S.E. (shaded area) in **F** and with a bar and error bars in **G**.

CT_{max} precedes the brain-wide depolarization

Since agar-embedded larvae experienced a brain-wide depolarization at temperatures close to the upper thermal limit of zebrafish, we asked whether the depolarization preceded, or co-occurred with, the loss of response observed during heat ramp in freely swimming fish. To do so, we simultaneously measured CT_{max} and neural activity in freely swimming zebrafish during a heat ramp, using epifluorescence imaging (**Figure 3A**, **B**, (Muto *et al.*, 2017)). CT_{max} (40.9±0.2°C) preceded the brain-wide depolarization (41.4±0.2°C, **Figure 3C**) in all individuals by 0.5°C on average (linear mixed-effects model, β±S.E.=0.5±0.1, $t_{(6)}$=4.5, p=0.004, R^2=0.3, **Figure 3D**). These results from freely swimming fish show that brain-wide depolarizations were not an artefact due to agarose embedding in the previous experiment (**Figure 2**) and that the brain-wide depolarization does not precede CT_{max}.

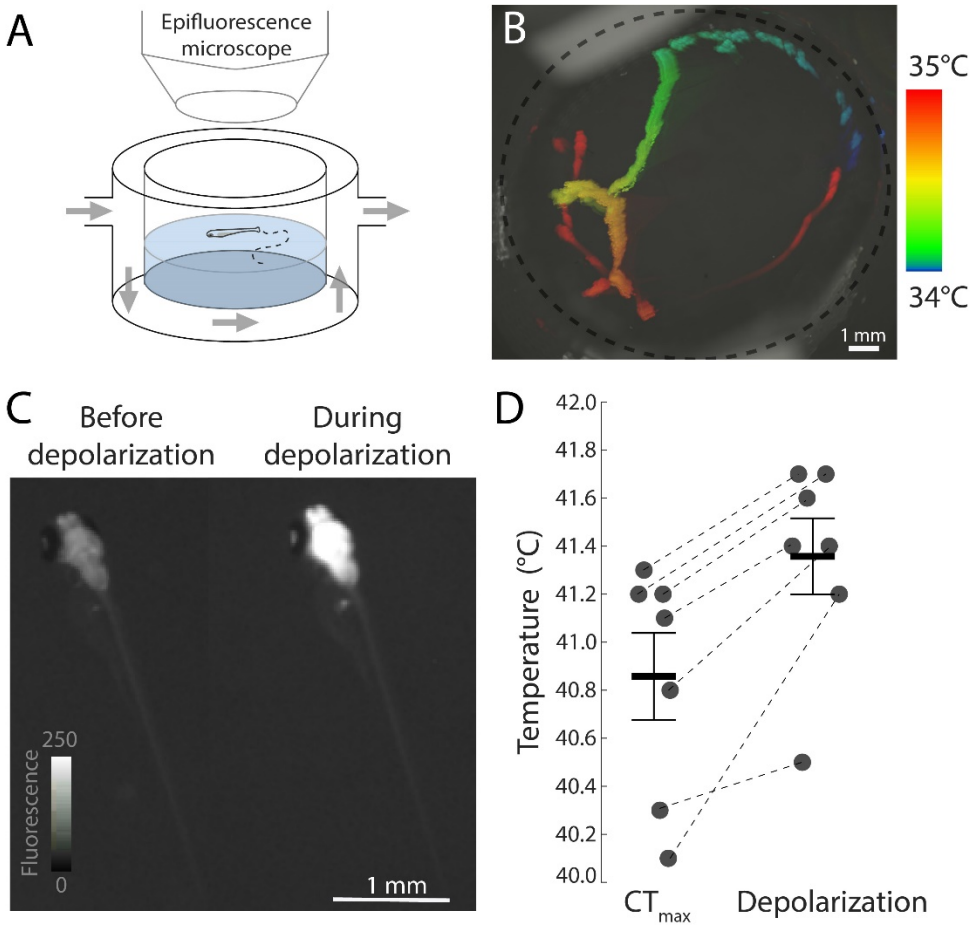

Figure 3. CT_{max} shortly precedes the brain-wide depolarization in freely swimming zebrafish larvae. **A.** Schematic overview of the experimental setup for calcium imaging in freely swimming five-day-old *Tg(elavl3:GCaMP6s)* zebrafish larva. **B.** Top view of setup with colour-coded time projection of a heat ramp fish's movements in the set-up for three minutes (34-35°C). **C.** Representative images of brain fluorescence in the same fish as in **B**, before (left) and during (right) the brain-wide depolarization. **D.** CT_{max} and depolarization onset temperatures measured in heat ramp fish (black circles, n=7; linear mixed effects model: β±S.E.=0.5±0.1, $t_{(6)}$=4.5, p=0.004, R^2=0.3, **Table S3**). The bars and error bars indicate the mean and S.E. of the CT_{max} and depolarization measurements.

Cardiac function declines before CT_{max} and the brain-wide depolarization

Hypoxic brain tissues due to a cardiorespiratory limitation, could result in neural dysfunction during heat ramping. We therefore simultaneously measured neural activity and heart-beat frequency in the same fish during a heat ramp (**Figure 4A**, **B**) to test if the heart rate was altered prior to the depolarization onset. When the temperature was increased from 28°C to 34°C, the heart rate increased with a mean Q_{10} value of 1.9, from 4.4±0.1Hz to 5.7±0.1Hz (linear mixed-effects model: β±S.E.=1.3±0.2Hz, $t_{(36)}$=6.9, p<0.001, R^2=0.8 **Figure 4C**). From 34 to 37°C, the heart rate decreased by 16% to 4.7±0.2Hz (β±S.E.=0.9±0.2, $t_{(36)}$=-4.9, p<0.001) and then remained stable during the period preceding the brain-wide depolarization (β±S.E.=-0.1±0.2, $t_{(36)}$=0.6, p=0.6**, Figure 4C**). We also examined whether heart rate was affected during the

brain-wide depolarization but it was unchanged (**Figure 4D**, **E**). When the fish were returned to normal holding temperature after the brain-wide depolarization the heart rate decreased by 34% from 4.7±0.2Hz to 3.1±0.3 Hz (β±S.E.=1.6±0.2 Hz, $t_{(36)}$=-8.5, p<0.001, **Figure 4C**). Altogether, our data shows a decline in cardiac activity during the heat ramp, but no abrupt change in cardiac function prior to the depolarization onset, during the period when CT_{max} occurs.

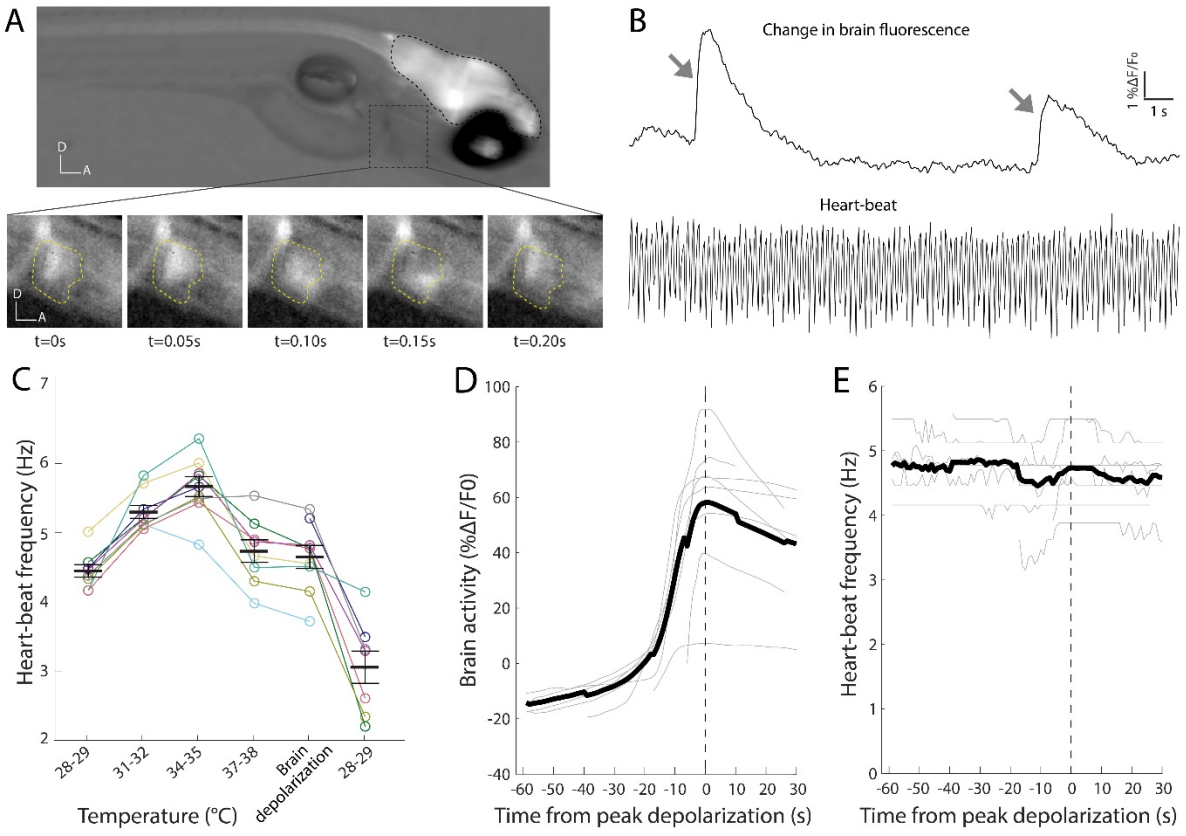

Figure 4. Heart rate before and during brain-wide depolarization in embedded larval zebrafish. **A**. Top panel: representative example of simultaneous neural activity and heartbeat imaging in a five-day-old *Tg(elavl3:GCaMP6s)* zebrafish larva embedded laterally in agar, using epifluorescence microscopy. The brain is outlined with black dashed lines and the heart with a dashed grey square (top panel). Bottom panel: The heart region (dashed yellow line) is shown in inverted grayscale (D=dorsal, A=anterior) during a beating cycle. **B**. Top panel: change in brain fluorescence (% $\Delta F/F_{0,}$) in the same fish as in **A**, at 31°C. Calcium events are indicated by grey arrows. Bottom panel: change in luminosity within a region of interest in the heart during the same period, which is used to calculate the heartbeat frequency. **C**. Average heartbeat frequency in embedded heat ramp fish (n=10), recorded at different temperature intervals. The x-axis shows ranges of 1°C elevation during which the heartbeat was measured. The fifth temperature category (brain depolarization) corresponds to heartbeat frequency during the 60 seconds pre- and the 30 seconds post-peak brain depolarization. The sixth category corresponds to heartbeat frequency after fish were rapidly returned to holding temperature. Horizontal bars and error bars indicate the mean and S.E. of the heartbeat value for each temperature range. Individual fish are colour-coded (linear mixed effects model: R^2= 0.8, **Table S4**). Change in neural activity (**D**) and heartbeat frequency (**E**) during the brain-wide depolarization (same period as "Brain depolarization" in **C**). Thin grey lines represent individual fish and the thick black line represent the mean. All traces are aligned with respect to the peak fluorescence (vertical dashed line).

Oxygen availability modulates temperature for CT_{max} and brain-wide depolarization

Since the heart rate is only 4-5 Hz at the time of the brain-wide depolarization (**Figure 4C** and **4E**), it is possible that the cardiorespiratory system cannot match the increasing oxygen demand of the neural tissue. If oxygen availability limits thermal tolerance, we expect that oxygen manipulations during heat ramping would alter CT_{max} and neural function.

To test the effect of oxygen availability on CT_{max}, we first measured the temperature at loss of response in freely swimming larvae zebrafish exposed to hypoxic and hyperoxic conditions during heat ramping, at 60 and 150% oxygen of air-saturated water respectively. Both treatments had on average a lower CT_{max} than in the previous experiment (**Figure 1E**) likely due to experimental differences. The average CT_{max} occurred 0.9°C lower in hypoxia (39.2±0.1°C) than in hyperoxia (40.1±0.3°C; linear regression model, β±S.E.=0.9±0.3°C, $t_{(26)}$=3.2, p=0.004; $F_{(1,26)}$=10.2, R^2=0.3; **Figure 5A**), which indicates that oxygen availability affects behavioural thermal tolerance in larval zebrafish.

To test the effect of oxygen availability on neural activity, agar-embedded fish were placed under an epifluorescence microscope and subjected to three oxygen treatments during heat ramping: hypoxia, normoxia and hyperoxia at 60, 100 and 150% oxygen of air saturated water, respectively. The brain-wide depolarization occurred at 40.7±0.4°C in normoxia. It occurred 1.8°C lower in the hypoxia (38.8±0.2°C; linear regression model, β±S.E.=-1.8±0.4, $t_{(20)}$=-4.8, p<0.001; $F_{(2,20)}$=40.4, R^2=0.8; **Figure 5B**). On the contrary, the hyperoxia treatment during heat ramping increased the depolarization temperature by 1.3°C compared to normoxia (42.0±0.2°C; β±S.E.=1.3±0.4, $t_{(20)}$=3.3, p=0.003). These results indicate that oxygen availability strongly influences the onset of brain-wide depolarization in larval zebrafish.

To further determine the effect of oxygen availability on neural activity when zebrafish reach their upper thermal limits, we calculated the frequency of brainstem calcium events during the 15 minutes before the brain-wide depolarization. Neural activity in the locomotor brain center sharply decreased at high temperature in all treatments: almost no calcium events were detected during the minutes preceding the depolarization (**Figure 5C**). The hyperoxia group retained a higher event frequency than the hypoxia and control groups at the start of this period (linear mixed-effects model, time: β±S.E.=0.08±0.02, $t_{(216)}$=3.9, p<0.001; hyperoxia*time: β±S.E.=0.09±0.03, $t_{(216)}$=3.3, p=0.001; R^2=0.3, **Figure 5C**). This indicates that increased oxygen availability partially rescued neural function near zebrafish upper thermal limit.

We also observed an effect of oxygen availability on the temporal dynamic of the brain depolarization. Oxygen availability did not change the amplitude of the brain-wide depolarization (normoxia: 88.2±17.6%$\Delta F/F_0$; linear regression model, hypoxia: β±S.E.=-3.1±17.1, $t_{(20)}$=-0.2, p=0.86; hyperoxia: β±S.E.=-15.4±17.4, $t_{(20)}$=-0.9, p=0.39; $F_{(2,20)}$=0.5, R^2=-0.05, data not shown). However, oxygen availability significantly improved the depolarization recovery time. Compared to the normoxia group, the hyperoxia group returned to baseline activity after the depolarization 1.3 minutes faster, and the hypoxia group 2 minutes slower (recovery time in normoxia: 3.0±0.4 min; linear regression model, hypoxia: β±S.E.=2.0±0.5, $t_{(19)}$=4.1, p<0.001; hyperoxia: β±S.E.=-1.3±0.5, $t_{(19)}$=-2.5, p=0.02; $F_{(2,19)}$=0.5, R^2=0.7, **Figure 5D-E**).

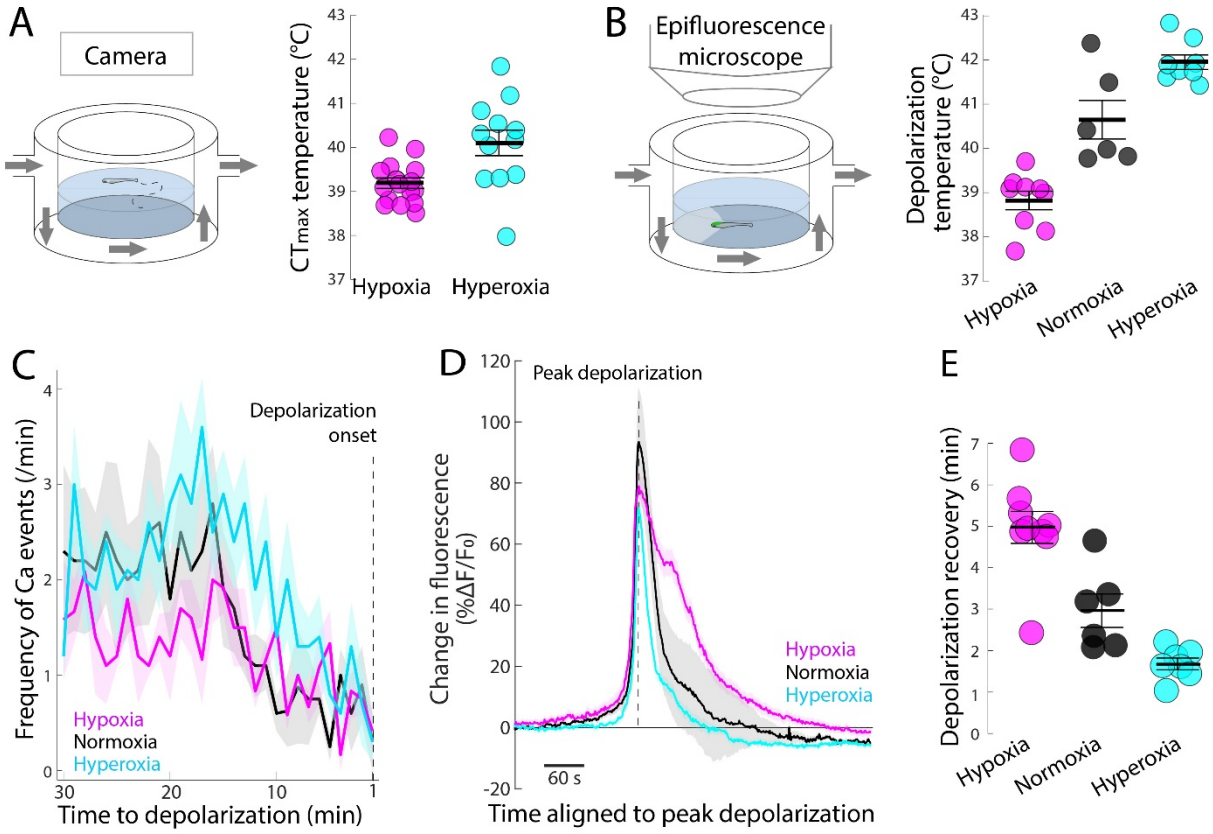

Figure 5. Oxygen availability affects both CT_{max} and depolarization onset temperatures.
A. Effect of oxygen availability on CT_{max} measured in freely swimming fish (set-up illustrated in left panel) during heat ramping with water oxygen set at 60% (hypoxia, magenta circles, n=16) or 150% (hyperoxia, cyan circles, n=12) of air saturated water (right panel; linear regression model: β±S.E.=0.9±0.3, $F_{(1,26)}$=10.2, p=0.004, R^2=0.3, **Table S5**). **A-E.** All results for hypoxia (60%, magenta), normoxia (100%, black) and hyperoxia (150%, cyan) are presented with mean and S.E. (**A**, **B**, **E**: bars and error bars; **C**, **D**: solid lines and shaded area). **B.** Brain-wide depolarization onset temperatures measured in agar-embedded *Tg(elavl3:GCaMP6s)* five-day-old fish (set-up illustrated in left panel) during heat ramping in hypoxia (n=9), normoxia (n=6) and hyperoxia (n=8; linear regression model, hypoxia: β±S.E.=-1.8±0.4°C, $t_{(20)}$=-4.8, p<0.001; hyperoxia β±S.E.=1.3±0.4°C, $t_{(20)}$=3.3, p=0.003; $F_{(2,20)}$=40.4, R^2=0.8, **Table S6**). **C.** Frequency of brainstem calcium events recorded during the 30 minutes preceding the brain-wide depolarization in hypoxia (n=5), normoxia (n=5) and hyperoxia (n=6; linear mixed-effects model for the last 15 minutes, time: β±S.E.=0.08±0.02, $t_{(216)}$=3.9, p<0.001; hyperoxia*time: β±S.E.=0.09±0.03, $t_{(216)}$=3.3, p=0.001; R^2=0.3, **Table S7**). **D.** Change in brain fluorescence aligned to the peak

depolarization in hypoxia (n=9), normoxia (n=6) and hyperoxia (n=8). **E.** Recovery time between peak depolarization and the return to baseline fluorescence in hypoxia (n=9), normoxia (n=6) and hyperoxia (n=7; linear regression model, hypoxia: β±S.E.=2.0±0.5, $t_{(19)}$=4.1, p<0.001; hyperoxia: β±S.E.=-1.3±0.5, $t_{(19)}$=-2.5, p=0.02; $F_{(2,19)}$=0.5, R^2=0.7, **Table S7**).

DISCUSSION

A massive heat-induced global depolarization arose in the larval brain, at similar temperatures as CT_{max} occurred in freely swimming fish. These brain depolarizations were 4-5 times the magnitude of brainstem locomotor calcium events, and lasted much longer (**Figure 2**). This abnormally high neural activity in response to heat stress is reminiscent of heat-induced seizures (Dube *et al.*, 2000; Shinnar & Glauser, 2002; Hunt *et al.*, 2012), and of heat-induced spreading depolarizations (Jørgensen *et al.*, 2020), which are slow propagating waves of brain depolarization (Spong *et al.*, 2016). The temporal dynamic of the events measured here is characteristic of the latter. First, the depolarizations spread slowly across the brain (**Figure 2E**), at a speed consistent with that reported for spreading depolarizations (2-9 mm/min, (Woitzik *et al.*, 2013; Spong *et al.*, 2016)), and slower than seizures (Wenzel *et al.*, 2017; Liu & Baraban, 2019). Second, the long post-depolarization recovery time (**Figure 5E**) is consistent with that seen after spreading depolarizations (Sawant-Pokam *et al.*, 2016; Spong *et al.*, 2016), and it is much longer than that measured after brain seizures (a few seconds, (Diaz Verdugo *et al.*, 2019; Liu & Baraban, 2019)). Overall, the temperatures at which these spreading depolarizations occurred, as well as their transient nature, made it a plausible candidate to explain the prolonged, yet reversible unresponsive state that we observed at CT_{max}.

If upper thermal tolerance in zebrafish larvae is caused by a spreading depolarization shutting down central nervous system function, the depolarization should precede or coincide with CT_{max} measured in the same animal. Surprisingly, larval zebrafish reached CT_{max} *before* they developed a brain-wide depolarization. This is in contrast with a series of studies in insects in which measures of upper thermal tolerance correlated with the onset of spreading depolarization in the central nervous system (Andersen *et al.*, 2018; Jørgensen *et al.*, 2020). In these studies, upper thermal limits and spreading depolarization onsets were measured in separate individuals, respectively freely moving flies and central nervous system preparations. Using a similar approach in the first part of this article, we also found overlapping temperature ranges for CT_{max} and spreading depolarization onset. Only when measuring both parameters within the same individual could we resolve the small but consistent difference between these consecutive events (**Figure 3D**), and determine that CT_{max} preceded spreading depolarization. We thus conclude that spreading depolarization is not the cause of CT_{max} in zebrafish.

The fact that CT_{max} precedes the spreading depolarization does not rule out neural impairment as a possible mechanism determining the upper thermal limit. Previous studies suggested that neural function is impaired during acute heat stress due to either a direct effect of temperature (Friedlander et al. 1975; Jutfelt et al. 2019), or due to heat-induced tissue hypoxia. Extracellular recordings of the pyloric neuron in the crab stomatogastric nervous system show that the characteristic rhythmic firing crashes at high temperatures (Marder *et al.*, 2015). Similarly, extracellular recordings of cerebellar neurons in anesthetized goldfish indicate a sharp decrease in spontaneous and sensory-evoked firing rates at high temperatures (Friedlander *et al.*, 1976). In addition, a strong reduction in spontaneous neural activity occurs in ischemic brain tissue in rodents (Buzsaki *et al.*, 1989; Barth & Mody, 2011) and in oxygen-deprived cultures of human cortical neurons (le Feber *et al.*, 2016). Such findings indicate that both direct effects of temperature and tissue hypoxia are plausible candidate mechanisms. In line with these previous studies, we found that neural activity was strongly reduced in locomotor brain regions during the minutes preceding the depolarization (**Figure 2 and 5C**), which we interpret as an early indication of neural malfunction that underlies the degradation of zebrafish locomotion observed during the corresponding period (**Figure 1C-D**). As this period of neural inactivity in the minutes leading up to CT_{max} could be due to both direct impacts of temperature and/or oxygen deficit on neural function, we manipulated oxygen water concentrations to test if oxygen availability alters CT_{max} and neural function.

We found that hyperoxia (150% air saturation) improved both behavioural and neural thermal resilience compared to hypoxia. The fact that neural activity in the locomotor brain centre was more resilient to high temperature in hyperoxia than in hypoxia and normoxia provides a likely mechanism for the improved behavioural resilience of zebrafish in hyperoxic conditions. Furthermore, similarly to earlier measurements in normoxia, neural activity was strongly silenced in the brainstem of fish during the very last minutes preceding the brain depolarization, when fish reach their upper thermal limit (**Figure 3D**). This shows that central nervous function impairment coincided with the temperatures where CT_{max} occurs, further suggesting that neural impairment due to a cumulative lack of oxygen and/or accumulation of anaerobic metabolites contributes to the unresponsive state observed at the upper thermal limit.

A few studies have found a positive effect of increased oxygen availability on thermal tolerance, while most fail to find an effect of hyperoxia (McArley *et al.*, 2020). Hyperoxia improved the upper thermal limit by 1.1 °C (loss of equilibrium) in the European perch (Ekström *et al.*, 2016) and in the Common triplefin (McArley *et al.*, 2018). Increased aquatic

364 oxygen availability also extended the survival of several ectotherm species (arthropods,
365 chordates, echinoderms, molluscs, and fish) at extreme high temperatures (Verberk *et al.*, 2018;
366 Giomi *et al.*, 2019). However, hyperoxia did not improve thermal tolerance for a large number
367 of other fish species (McArley *et al.*, 2020). Moreover, the upper thermal limit of the red drum
368 and lumpfish was only reduced under severe hypoxic conditions (Ern *et al.*, 2016).
369 Additionally, the aerobic scope, the aerobic capacity available for non-maintenance activities,
370 remains high in some ectotherms at thermal limits, indicating surplus oxygen transport capacity
371 (Overgaard *et al.*, 2012; Grans *et al.*, 2014; Wang *et al.*, 2014; Brijs *et al.*, 2015; Ekström *et*
372 *al.*, 2016). Taken together these studies suggest that oxygen limitation is not a general
373 mechanism limiting thermal tolerance across all species and contexts. Our results suggest that
374 inter-species differences in neural tissue resilience to heat and oxygen deprivation might be a
375 critical physiological factor explaining these different reports. It will also be interesting to
376 investigate whether the sensitivity of CT_{max} to oxygen availability in zebrafish is limited to
377 early life stages or persists throughout ontogeny.

378 To test whether heat ramping causes cardiac dysfunction we examined heart rate and brain
379 activity simultaneously. The heart rate initially (from 28-34°C) increased as expected with
380 temperature, similar to previous reports (Gollock *et al.*, 2006; Farrell, 2007). This initial
381 increase was followed by a decrease to to 270 beats per minute, a heart rate then sustained upon
382 further heating and throughout the brain depolarization. Similarly, a decrease or plateau in heart
383 rate with increasing temperatures has been reported for salmonids (Farrell, 2009), and
384 European perch (Ekström *et al.*, 2016). The lack of heart rate increase when approaching
385 thermal limits might contribute to mismatch between oxygen delivery and metabolic rate. Such
386 a mismatch may have caused developing tissue hypoxia and accumulation of metabolites,
387 which could have contributed to causing the loss of responses at CT_{max}.

388 Animals are adapted to widely different climates, and because of this, the temperatures at which
389 heat-induced behavioral alterations occur are strongly species-specific. Yet, the sequence and
390 nature of heat-induced behavioral alterations seem relatively well conserved across species.
391 For example, a similar sequence of events occur in fruit fly and goldfish subjected to rapidly
392 increasing temperatures: hyperactivity, then loss of coordinated movement, followed by loss
393 of equilibrium, before entering into a heat-coma indicated by an animal lying still and
394 unresponsive to mechanical stimulations (Friedlander *et al.*, 1976; Jørgensen *et al.*, 2020).

395 To enable comparison with previous studies we quantified the behavioral changes that occurred
396 during heat ramping. Although the swimming velocity of heat ramp fish tended to be higher

than that of controls between 31-38 degrees, there was no clear period of heat-induced hyperactivity, possibly due to the high interindividual variability in locomotion in larval zebrafish. Loss of motor coordination (spiral swimming) and loss of equilibrium occurred in most heat ramp larval zebrafish, followed by a state of unresponsiveness that was similar to the heat-coma documented in goldfish and fruit flies. The loss of response endpoint used here was stable throughout larval development and yielded results within the range recorded using the loss of equilibrium criterion in adults of the same *Tg(elavl3:GCaMP6s)* line (**Figure 1E**), or in wild-type adult zebrafish (Morgan *et al.*, 2018), thus supporting its use a criterion for CT_{max} in larvae. In addition, spiral swimming could be used as a novel, specific and early sign of heat-induced locomotor dysfunction before the upper thermal limit is reached.

In conclusion, we show that the acute thermal limits of larval zebrafish are not caused by global brain depolarization, but are instead related to a drop in neural acivity preceding CT_{max}. Furthermore, in concordance with OCLTT predictions, tissue oxygen availability appears to constrains both brain function as well as the whole animal thermal limits during thermal ramping.

METHODS

Animals and housing

Experiments were conducted on five- to ten-day-old larvae and seven- to ten-month-old zebrafish (*Danio rerio*). The transgenic line *Tg(elavl3:GCaMP6s)* (Vladimirov *et al.*, 2014) in *nacre/mitfa* background (Lister *et al.*, 1999) was used. Eggs were collected in the morning and kept at a density of one per mL in fish water (0.2g of marine salt and 0.04 L AquaSafe per litre of carbon-filtrated water, used for all experiments). After hatching at three days post-fertilization, the larvae were kept in small nursery tanks and fed twice a day with larval food (Tetramin, Tetra) after 5 days post-fertilization. Fish were maintained under standard laboratory conditions (26.8 ± 0.1°C; 12/12-hour light/dark cycle). On the day of the experiment, the fish were fed once after the experiment was finished. All experimental procedures performed on zebrafish were in accordance with the 2010/63/EU directive and approved by the Norwegian Animal Research Authority (Food and Safety Authority; Permit number: 8578).

The experiments consisted of five parts performed on different fish: 1) measuring CT_{max} in freely swimming zebrafish larvae, 2) recording brain activity during warming in agar-

429 embedded zebrafish larvae, 3) simultaneous recording of CT_{max} and depolarization in freely
430 swimming zebrafish larvae, 4) simultaneous recording of heart rate and brain activity during
431 heat ramping and 5) recording of CT_{max} and neural function under oxygen manipulation during
432 warming.

433

434 **CT_{max} in freely swimming larvae**

435 *CT_{max} setup*

436 Larval zebrafish swam in the behavioural arena (central compartment) of a double-walled glass
437 heating-mantle made in the NTNU glass workshop. The dimensions were as follows: outer
438 diameter= 42 mm, inner diameter= 29 mm, outer height= 32 mm, inner height= 19 mm. The
439 fish movement was recorded using a webcam (Logitech C270, 720p) positioned above the
440 arena. The arena was placed above a background illumination light source to enhance contrast.
441 Two outlets connected the glass heating mantle to a water bath. Adjustment of water
442 temperature of the arena was achieved by pumping water from an external heating bath through
443 the heating-mantle surrounding the arena. The heating rate in the arena was 0.3°C per minute
444 as described in Morgan et al., (2018). The water temperature inside the central chamber of the
445 arena was recorded at 1 Hz using two thermocouples (type K, Pico Technology) connected to
446 a data logger (TC-08, Pico Technology).

447 *CT_{max} assay*

448 The arena was filled with three mL of 28°C water supplied with air bubbling through a
449 modified hypodermic needle fixed to the side wall of the compartment. At the beginning of a
450 CT_{max} recording, a single larva was carefully transferred to the arena. All individuals were
451 given 15 minutes to habituate to the arena before the recording started. The CT_{max} assay lasted
452 up to 50 minutes, during which the temperature within the arena increased from 28°C by
453 0.3°C/min until the larvae reached CT_{max}. The temperature was kept constant at 28°C for
454 recordings of control fish. The fish behaviour was recorded at 4-7 Hz during four intervals: 28-
455 29°C, 31-32°C, 34-35°C and 37°C-CT_{max}. For control larvae, recordings of matching durations
456 were taken at corresponding time points. Methods commonly used to determine CT_{max} in fish
457 were unsuitable for 5 dpf larvae zebrafish: loss of equilibrium (Morgan *et al.*, 2018) also
458 occurred in control fish without heat ramp; and muscular spasms (Lutterschmidt & Hutchison,
459 2011) could not be reliably quantified due to the larvae's small size. Thus, CT_{max} was
460 determined as the temperature at which the animal became unresponsive (Friedlander *et al.*,
461 1976; Sherman & Levitis, 2003; Jørgensen *et al.*, 2020), which was defined as the first of three

consecutive tactile stimulations that did not elicit an escape response (loss of response). The stimulations were applied to the larva's trunk using the tip of a capillary micro-ladder (VWR), with a minimum of three seconds between consecutive stimulations. Upon CT_{max}, the fish was transferred to 28°C water and visually monitored. Fish that did not recover normal locomotor activity were rapidly euthanized and were not included in the analysis (this happened in only four out of 44 fish, similar to previous reports (Morgan *et al.*, 2018; Åsheim *et al.*, 2020)).

CT_{max} assay in adult zebrafish

To compare CT_{max} throughout development, 16 adult Tg(elavl3:GCaMP6s) zebrafish, aged seven- to ten-month-old, were tested in the CT_{max} setup described by Morgan et al., (2018). The fish were tested in groups of eight fish in a rectangular acrylic tank (25 cm long, 20 cm wide, 18 cm deep) filled with nine litres of water. Individual CT_{max} was measured at the temperature of loss of equilibrium determined as two seconds of inability to maintain postural stability (Morgan *et al.*, 2018). The fish were removed immediately after the criterion was reached. All animals survived the test.

CT_{max} assay data analysis

The fish position was manually detected in MATLAB (MathWorks 2018) at 28-29°C, 31-32°C, 34-35°C, 37-38°C and during the 1°C elevation preceding CT_{max}. The average speed was calculated during these intervals. Loss of equilibrium and spiral swimming events were manually labelled by an experimenter during the 12 min preceding CT_{max} in heat ramp fish, and during the corresponding period in control fish. Loss of equilibrium was recorded when the fish tilted to the side for at least one second (**Movie S2**). Spiral swimming event was recorded when the fish rapidly performed a minimum of two consecutive revolutions with diameter below 5 mm (**Movie S1**).

Brain activity during warming in agar-embedded larvae

The calcium imaging to record brain activity during warming was executed using the same double-walled glass heating mantle as described for the CT_{max} assay above.

Epifluorescence calcium imaging in agar-embedded zebrafish larvae

For the imaging of neural activity in embedded fish (**Figure 2A**, **B**), a five-day-old larva was embedded at the bottom of the central glass compartment in 2% low-gelling temperature agarose (Merck). The agarose was carefully removed around the eyes and mouth upon hardening and the arena was filled with 3 mL water. Calcium fluorescence was recorded with a custom-made epifluorescence microscope equipped with a 10x water-immersion objective

(UMPLFLN, Olympus), a set of GFP emission-excitation filters (FGL400, MD498, MF525-9, Thorlabs) and a mounted blue LED controlled by a driver (MWWHL4, LEDD1B, Thorlabs). Images were collected at 5 Hz via a custom-written Python script using the Pymba wrapper for interfacing with the camera (Mako G319B, Allied vision).

Simultaneous recording of CT_{max} and depolarization in freely swimming larvae

Calcium imaging in freely swimming fish was used to record CT_{max} and brain-wide depolarization in the same individuals during one trial. For the imaging of freely swimming fish, the double-walled glass heating-mantle was placed under an epifluorescence microscope (AxioImager, ZEISS) equipped with a megapixel camera (AxioCam 506, ZEISS). The larva was swimming at the centre of the arena, within a 13 mm diameter region delimited with a nylon mesh, to match the limited field of view of the microscope (14 x 14 mm). Time-lapse of fluorescent images were recorded at 5 Hz using the Zen software (ZEN Lite Blue, ZEISS). Since the recordings were made in the dark, the experimenter watched the live recording display of the recording on the computer screen to visually guide the pokes to the fish tail. The nylon mesh created a small thermal gradient in the arena from the central part to the outer area outside the mesh. During the experimental trials, the temperature was recorded outside the mesh to ensure a full view of the fish. The temperature gradient was thoroughly quantified in an additional experiment over six heat ramps, by recording the temperature in the arena centre and outside the mesh near the outer wall of the arena with two thermocouples at each location. The gradient was accounted for to calculate the water temperature the fish was exposed to.

Calcium imaging data analyses

Calcium imaging recordings on embedded fish were corrected for slow drift due to agarose expansion using the Fiji's (Schindelin *et al.*, 2012) Template matching plugin (*Align slices in stack*). The regions of interest corresponding to the whole brain, the telencephalon and the brainstem were manually segmented. The raw calcium fluorescence signal was calculated by averaging all pixels within a region. To reproducibly detect the brain-wide depolarization onset time across fish, the whole brain raw fluorescence signal was first processed to filter out the calcium events using a 2^{nd} order Butterworth filter (low pass, 0.01 Hz cut-off frequency). The average value and standard deviation of the filtered trace's time derivative were calculated during the 17 min preceding the approximate onset of the depolarization. The depolarization onset was set when the time derivative exceeded the average baseline value by more than five standard deviation. For calcium event detection during the period preceding the brain-wide depolarization, the fluorescence change was calculated for each brain region using a sliding

window of the previous two minutes. The calcium events were detected automatically using the MATLAB function *findpeak*.

Measuring brain-wide fluorescence during the freely swimming fluorescence assay was cumbersome due to the fish moving and tilting. Thus, the depolarization onset temperature was determined by two investigators, who independently selected the time at which the fluorescence increased abruptly within the brainstem/diencephalon. The final depolarization onset value was obtained by averaging both estimates (agreement between experimenters: 19 ±4s out of 55 minutes).

Cardiac function and brain activity during heat ramping in agar-embedded larvae

Heat rate and neural activity were simultaneously recorded at 20 Hz in laterally mounted larvae, under an epifluorescence microscope (AxioImager, ZEISS) equipped with a megapixel camera (AxioCam 506, ZEISS). Recordings were aligned when needed using Fiji's Template matching plugin. Whole brain and heart regions of interest were selected in Fiji. Fish whose heart was out of focus during more than two recording intervals (1 fish out of 10), and frames where movement artefacts could not be corrected were not included in the rest of the analysis. Heartbeat frequency during a recording interval was calculated using Matlab's continuous wavelet transform function (cwt).

Oxygen effects on CT_{max} and neural function during warming

CT_{max} assay with oxygen level manipulation

The CT_{max} setup described earlier was used to record the effect of oxygen manipulation on CT_{max}. The arena was intermittently bubbled with pure oxygen or pure nitrogen to increase or decrease oxygen levels, respectively. The bubbling flow rate was manually adjusted using tubing clamps. A fibre optic oxygen probe (OXROB10, PyroScience) and a temperature probe (TSUB21, PyroScience) connected to an oxygen and temperature meter (FireSting O2, PyroScience) were placed in the chamber to monitor and record the oxygen levels during the assay. The oxygen saturation level was displayed in real time using an oxygen logger software (pyro oxygen logger, PyroScience) and kept at 150 %, or 60%, of air saturation during the whole CT_{max} assay by manually adjusting the bubbling intensity.

Recording neural activity with oxygen level manipulation

The epifluorescence calcium imaging setup for embedded fish was used to measure neural activity during heat ramping with oxygen manipulation. Fish were visually stimulated using pulses of red light (2 second long, every 30 second) using a red LED positioned in front of the

fish. For control treatment, the water was bubbled with air through a modified hypodermic needle and maintained at 100% oxygen of air saturation during the trials. To increase the oxygen level during oxygen manipulation trials, oxygen was gently blown on the surface. To decrease oxygen saturation, the water was bubbled with nitrogen. A bare fibre microsensor (OXB430, PyroScience) and a temperature probe (TDIP15, PyroScience) were placed in the chamber to monitor and record oxygen levels. Oxygen levels were adjusted to either 150%, or 60%, of air saturated water during the high and low oxygen treatments, respectively.

Calcium imaging data analyses

Depolarization onset (**Figure 5B**) and brainstem calcium events (**Figure 5C**) were calculated as described above. For calcium events, fish in which the brainstem signal was weak and noisy due to uneven mounting were not included in the analysis. One fish in the hyperoxic group could not be included in the calculation of the recovery time (**Figure 5E**) because the recording ended before the fluorescence reached baseline after the depolarization.

Statistical analyses

Data are reported in the text as mean and standard error (S.E.), unless stated otherwise. All statistical analyses were conducted in R version 4.0.2 (R Core Team, 2020). We used linear regression models on independent measurements and the assumptions of normality for homoscedasticity of residual variance were assessed visually using residual plots. Alternative models were considered if assumptions were violated. For responses recorded as repeated measures on individual fish linear mixed-effects models were created using the *lmer* function from the *lme4* package v.1.1-23 to account for fish identity as random effect. Akaike information criterion was used to consider interactions in models with two predictor variables and model assumptions were visually assessed using residual plots. The effects of predictor variables are presented with effect size (β), their S.E. estimated by the respective models and the R^2 for the fixed effects is presented. The significance of effects was considered with a *p*-value criterion of $p<0.05$.

CT_{max} and behavioural response to heat ramping

To analyse the swimming velocity during heat ramping and in the control group a linear mixed-effects model was performed with treatment and time step as predictor variables and the fish identity as random factor. No interaction was included (ΔAIC=2). **Table S1** is a summary of the model results and **Figure S1** displays the datapoints. The proportion of spiral swimming

events was analysed using a Chi-square test to handle the lack of variance in the control group. A Wilcoxon rank sum test was used to test the treatment effect on loss of equilibrium response. To test the difference in CT_{max} throughout development, a linear regression model was used with CT_{max} as a function of the age. The CT_{max} value of one adult fish was an extreme outlier and was not included in the analysis. Results from models with and without this fish are included in the supplements (**Table S2**).

Temperature of CT_{max} and depolarization

The relationship between depolarization and CT_{max} response in freely swimming fish was analysed with a linear mixed-effects model with temperature as response variable, a categorical fixed effect of response type (CT_{max} or depolarization) and fish identity as a random factor (**Table S3**).

Change in cardiac function during heat ramping

Effect of temperature on heart rate was tested with a linear mixed-effects model where fish identity was defined as a random factor. The model was releveled to check for differences between the different temperature steps and the *p*-value significance criterion was accordingly reduced to $p<0.001$ for this analysis. Model results are presented in **Table S4**.

Effect of oxygen manipulation during on CT_{max} and depolarization

The effect of oxygen level on CT_{max} was analysed with a linear regression with CT_{max} as a function of the hypoxia and hyperoxia treatments. Two outliers and two fish who were euthanized after the assay were removed from the hyperoxic group. **Table S5** displays model results including these outliers. The effect of oxygen on neural activity was assessed using linear regression analyses. Depolarization temperature, amplitude of depolarization and recovery after depolarization were tested as functions of the treatment groups hypoxia, normoxia and hyperoxia. Frequency of calcium events for the 15 minutes preceding the brain-wide depolarization was analysed with an interaction between time and treatment. One extreme outlier in the hyperoxic group was excluded from the analyses. Results from models made with and without this fish are presented in **Table S6**.

Authors contributions

AHA, PH, FJ & FK conceived the project. FJ & FK jointly supervised. AHA, PH & FK built the experimental setups. AHA, PH, PK collected the data. FK wrote the software for data acquisition and analyses. AHA, PH & FK analysed the data, AHA and FK prepared the figures

623 and AHA performed the statistical analyses. AHA & FK wrote the manuscript, with
624 contributions from all authors.

625

626 **Acknowledgements**

627 The authors wish to thank the staff working at the animal facility for fish care, the members of
628 the Animal Physiology section at the Department of Biology for scientific discussions, and
629 Marius Mæhlum for the heartbeat frequency analysis code.

630

631 **Funding**

632 This work was supported by the Research Council of Norway (FK: FRIPRO grant 262698, FJ:
633 262942)

634

635 **SUPPLEMENT**

636

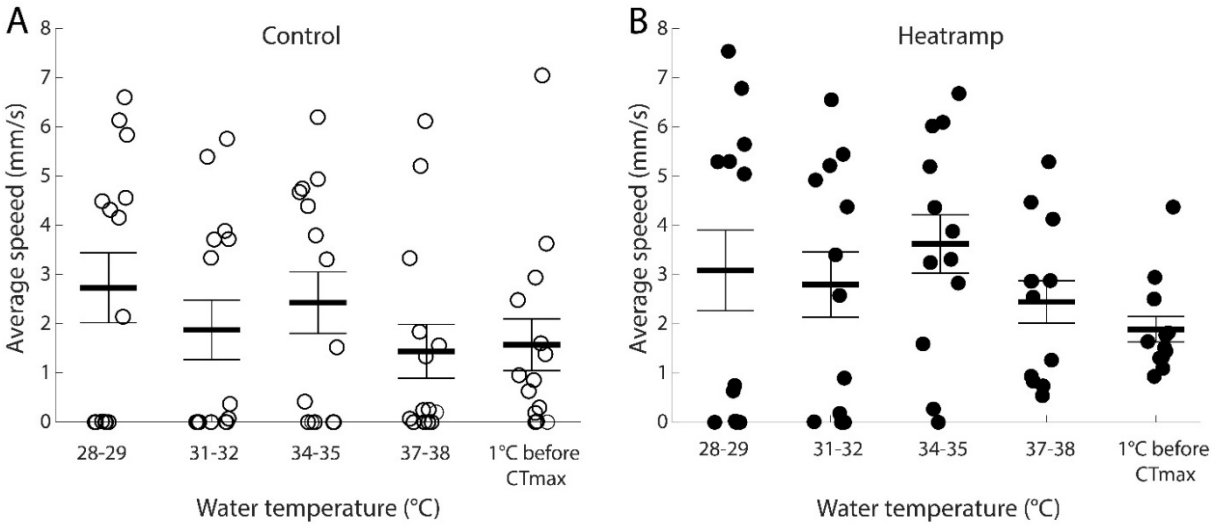

637

638 **Supplementary Figure S1**. Average swimming speed of (**A**) five-day-old control (n=14, empty circles) and (**B**)
639 heat ramp fish (n=12, black circles) as a function of temperature The swimming speed decreased from 2.9±0.4 to
640 1.7±0.5 mm/s during the assay. There was no difference in the change in swimming speed between the control
641 and the heat ramp treatment (linear mixed-effects model, time: β±S.E.=0.3±0.1, $t_{(103)}$=-2.5, p=0.013; treatment:
642 β±S.E.=0.8±0.6, $t_{(24)}$=1.2, p=0.23, **Table S1**). Bars and error bars represent mean and S.E, respectively.

643

644 **Supplementary Table S1.** Results of the statistical test for swimming speed in larval zebrafish (**Figure S1**) during
645 heat ramping (0.3°C/min) and over an equally long period for control fish (without heat ramping), testing the
646 effect of treatment and of time/temperature. The mixed-effects model includes fish identity as a random factor.
647 The control treatment is in the intercept and the units are in mm/s.

	Swimming speed			
Parameter	*Estimate (β)*	*S.E.*	*t-value*	*p-value*
Intercept (Control)	2.84	0.53	5.31	**<0.001**
Treatment (Heat ramp)	0.76	0.62	1.22	0.221
Time or temperature interval	-0.28	0.11	-2.53	**0.012**
Random Effects				
σ^2	3.08			
$\tau_{00\ FishID}$	1.88			
N_{FishID}	26			
Observations	130			
Marginal R^2 / Conditional R^2	0.056 / 0.414			

Supplementary Table S2. Results for the statistical test for CT_{max} in five-day-old, nine-day-old and adult zebrafish (**Figure 1E**) testing the effect of life-stage on the upper thermal limit. Model 1 is a linear regression model including all fish whereas in Model 2 one extreme outlier (<Q1-3*IQR) was removed from the adult group. The five-day-old group is in the intercept and units are in °C.

	Model 1				Model 2			
Parameter	*Estimate (β)*	*S.E.*	*t-value*	*p-value*	*Estimate (β)*	*S.E.*	*t-value*	*p-value*
Intercept (5dpf)	41.36	0.19	219.54	**<0.001**	41.36	0.17	250.19	**<0.001**
Age (9dpf)	-0.10	0.27	-0.39	0.698	-0.10	0.23	-0.45	0.659
Age (Adult)	-0.54	0.25	-2.16	**0.038**	-0.41	0.22	-1.84	0.073
Observations	40				39			
R^2 / R^2 adjusted	0.129 / 0.082				0.095 / 0.045			

Supplementary Table S3. Results of the statistical test on the relationship between CT_{max} and brain-wide depolarization (**Figure 3D**) testing the effect of event type on the recorded temperature. The mixed-effects model includes fish identity as a random factor. CT_{max} is in the intercept and units are in °C.

	CTmax and brain-wide depolarization			
Parameter	*Estimate (β)*	*S.E.*	*t-value*	*p-value*
Intercept (CTmax)	40.86	0.17	240.01	**<0.001**
Brain-wide depolarization	0.50	0.11	4.49	**<0.001**
Random Effects				
σ^2	0.04			
$\tau_{00\ FishID}$	0.16			
N_{FishID}	7			
Observations	14			
Marginal R^2 / Conditional R^2	0.249 / 0.840			

Supplementary Table S4. Results of the statistical test for the effect of temperature on heart rate in larval zebrafish (**Figure 4C**) recorded for 1 min intervals during heat ramping. The mixed-effects model includes fish identity as a random factor. The first temperature interval is in the intercept and the units are in Hz.

	Heart rate			
Parameter	*Estimate (β)*	*S.E.*	*t-value*	*p-value*
Intercept (28°C)	4.39	0.16	27.05	**<0.001**
Temperature (31°C)	0.91	0.18	4.92	**<0.001**
Temperature (34°C)	1.27	0.18	6.89	**<0.001**
Temperature (37°C)	0.36	0.19	1.91	0.057
Temperature (Depolarizaton)	0.26	0.18	1.40	0.161
Temperature (After)	-1.38	0.20	-6.98	**<0.001**
Random Effects				
σ^2	0.14			
$\tau_{00\ FishID}$	0.07			
$N_{\ FishID}$	9			
Observations	50			
Marginal R^2 / Conditional R^2	0.753 / 0.836			

Supplementary Table S5. Results of the statistical test for CT_{max} in hypo- and hyperoxia in larval zebrafish (**Figure 5A**) testing the effect of oxygen level on the upper thermal limit. Model 1 is a linear regression model excluding two extreme outliers (<Q1-3*IQR) from the hyperoxia group whereas Model 2 includes all fish. The hypoxia treatment is in the intercept and units are in °C.

	Model 1				**Model 2**			
Parameter	*Estimate (β)*	*S.E.*	*t-value*	*p-value*	*Estimate (β)*	*S.E.*	*t-value*	*p-value*
Intercept (Hypoxia)	39.19	0.19	209.48	**<0.001**	39.19	0.40	97.26	**<0.001**
Hyperoxia	0.91	0.29	3.19	**0.004**	0.08	0.59	0.14	0.888
Observations	28				30			
R^2 / R^2 adjusted	0.282 / 0.254				0.001 / -0.035			

Supplementary Table S6. Results of the statistical tests on 1) brain-wide depolarization onset, 2) amplitude of depolarization, and 3) recovery time after depolarization in norm-, hypo- and hyperoxia in larval zebrafish (**Figure 5B, D, E**) testing the effect of oxygen level on attributes of the brain-wide depolarization. The normoxic treatment (control) is in the intercept and units are in °C.

	Depolarization onset				**Amplitude of depolarization**				**Recovery time**			
Parameter	*Estimate (β)*	*S.E.*	*t-value*	*p-value*	*Estimate (β)*	*S.E.*	*t-value*	*p-value*	*Estimate (β)*	*S.E.*	*t-value*	*p-value*
Intercept (Control)	40.65	0.29	138.14	**<0.001**	88.17	13.22	6.67	**<0.001**	2.95	0.38	7.76	**<0.001**
Hypoxia	-1.83	0.38	-4.81	**<0.001**	-3.06	17.07	-0.18	0.860	2.02	0.49	4.10	**0.001**
Hyperoxia	1.30	0.39	3.34	**0.003**	-15.42	17.49	-0.88	0.389	-1.29	0.52	-2.49	**0.022**
Observations	23				23				22			
R^2 / R^2 adjusted	0.802 / 0.782				0.045 / -0.050				0.729 / 0.701			

Supplementary Table 7. Results of the statistical test for frequency of calcium events in norm-, hypo- and hyperoxia in larval zebrafish (**Figure 5C**) testing the effect of oxygen level on neural activity. The mixed-effects model includes an interaction between treatment and time and fish identity as a random factor. In Model 1 one fish from the hyperoxia treatment was excluded due to extremely high values during the last 15 minutes (>Q3-3*IQR) whereas Model 2 includes all fish. The normoxic treatment (control) is in the intercept and the units are in event/min.

	Model 1				**Model 2**			
Parameter	*Estimate (β)*	*S.E.*	*t-value*	*p-value*	*Estimate (β)*	*S.E.*	*t-value*	*p-value*
Intercept (Control)	0.30	0.23	1.30	0.195	0.30	0.34	0.89	0.371
Time	0.08	0.02	3.90	**<0.001**	0.08	0.03	3.05	**0.002**
Treatment (Hypoxia)	0.11	0.32	0.34	0.737	0.11	0.46	0.24	0.814
Treatment (Hyperoxia)	-0.07	0.33	-0.21	0.835	0.03	0.46	0.08	0.940
Time*Treatment (Hypoxia)	-0.00	0.03	-0.02	0.982	-0.00	0.03	-0.02	0.985
Time*Treatment (Hyperoxia)	0.09	0.03	3.25	**0.001**	0.12	0.03	3.46	**0.001**
Random Effects								
σ^2	0.53				0.87			
τ_{00}	0.11 $_{FishID}$				0.30 $_{FishID}$			
N	16 $_{FishID}$				17 $_{FishID}$			
Observations	235				250			
Marginal R^2 / Conditional R^2	0.332 / 0.447				0.307 / 0.484			

Supplementary Movie S1. Spiral swimming in a five-day-old zebrafish heat ramp larva. Speed 1X.

Supplementary Movie S2. Loss of equilibrium in the same heat ramp larva as in Supplementary Movie 1. Speed 1X.

Supplementary Movie S3. Representative illustration of the depolarization spreading in the brain of a five-day-old *Tg(elavl3:GCaMP6s)* larva exposed to a heat ramp (same fish as in Figure 2E). Speed 1X.

REFERENCES

Andersen, M.K., Jensen, N.J.S., Robertson, R.M., & Overgaard, J. (2018) Central nervous system shutdown underlies acute cold tolerance in tropical and temperate *Drosophila* species. *The Journal of Experimental Biology*, **221**, jeb179598.

Åsheim, E., Andreassen, A., Morgan, R., & Jutfelt, F. (2020) Rapid-warming tolerance correlates with tolerance to slow warming but not growth at non-optimal temperatures in zebrafish. *Journal of Experimental Biology*,.

Barth, A.M.I. & Mody, I. (2011) Changes in Hippocampal Neuronal Activity During and After Unilateral Selective Hippocampal Ischemia In Vivo. *Journal of Neuroscience*, **31**, 851–860.

Brijs, J., Jutfelt, F., Clark, T.D., Gräns, A., Ekström, A., & Sandblom, E. (2015) Experimental manipulations of tissue oxygen supply do not affect warming tolerance of European perch. *Journal of Experimental Biology*, **218**, 2448–2454.

Buzsaki, G., Freund, T.F., Bayardo, F., & Somogyi, P. (1989) Ischemia-induced changes in the electrical activity of the hippocampus. *Experimental Brain Research*, **78**.

Clark, T.D., Sandblom, E., & Jutfelt, F. (2013a) Aerobic scope measurements of fishes in an era of climate change: respirometry, relevance and recommendations. *Journal of Experimental Biology*, **216**, 2771–2782.

Clark, T.D., Sandblom, E., & Jutfelt, F. (2013b) Response to Farrell and to Pörtner and Giomi. *Journal of Experimental Biology*, **216**, 4495–4497.

Deutsch, C.A., Tewksbury, J.J., Huey, R.B., Sheldon, K.S., Ghalambor, C.K., Haak, D.C., & Martin, P.R. (2008) Impacts of climate warming on terrestrial ectotherms across latitude. *PNAS*, **105**, 6668–6672.

Diaz Verdugo, C., Myren-Svelstad, S., Aydin, E., Van Hoeymissen, E., Deneubourg, C., Vanderhaeghe, S., Vancraeynest, J., Pelgrims, R., Cosacak, M.I., Muto, A., Kizil, C., Kawakami, K., Jurisch-Yaksi, N., & Yaksi, E. (2019) Glia-neuron interactions underlie state transitions to generalized seizures. *Nature Communications*, **10**.

Dube, C., Chen, K., Eghbal- Ahmadi, M., Brunson, K., Soltesz, I., & Baram, T.Z. (2000) Prolonged febrile seizures in the immature rat model enhance hippocampal excitability long term. *Annals of Neurology*, **47**, 336–344.

Ekström, A., Brijs, J., Clark, T.D., Gräns, A., Jutfelt, F., & Sandblom, E. (2016) Cardiac oxygen limitation during an acute thermal challenge in the European perch: effects of chronic environmental warming and experimental hyperoxia. *American Journal of Physiology-Regulatory, Integrative and Comparative Physiology*, **311**, R440–R449.

Ern, R. (2019) A mechanistic oxygen- and temperature-limited metabolic niche framework. *Philosophical Transactions of the Royal Society B: Biological Sciences*, **374**, 20180540.

Ern, R., Huong, D.T.T., Phuong, N.T., Madsen, P.T., Wang, T., & Bayley, M. (2015) Some like it hot: Thermal tolerance and oxygen supply capacity in two eurythermal crustaceans. *Scientific Reports*, **5**, 10743.

Ern, R., Huong, D.T.T., Phuong, N.T., Wang, T., & Bayley, M. (2014) Oxygen delivery does not limit thermal tolerance in a tropical eurythermal crustacean. *The Journal of Experimental Biology*, 6.

Ern, R., Norin, T., Gamperl, A.K., & Esbaugh, A.J. (2016) Oxygen dependence of upper thermal limits in fishes. *Journal of Experimental Biology*, **219**, 3376–3383.

Farrell, A. p (2007) Cardiorespiratory performance during prolonged swimming tests with salmonids: a perspective on temperature effects and potential analytical pitfalls. *Philosophical Transactions of the Royal Society B: Biological Sciences*, **362**, 2017–2030.

Farrell, A.P. (2009) Environment, antecedents and climate change: lessons from the study of temperature physiology and river migration of salmonids. *Journal of Experimental Biology*, **212**, 3771–3780.

Friedlander, M.J., Kotchabhakdi, N., & Prosser, C.L. (1976) Effects of cold and heat on behavior and cerebellar function in goldfish. *J. Comp. Physiol.*, **112**, 19–45.

Genin, A., Levy, L., Sharon, G., Raitsos, D.E., & Diamant, A. (2020) Rapid onsets of warming events trigger mass mortality of coral reef fish. *PNAS*, **117**, 25378–25385.

Giomi, F., Barausse, A., Duarte, C.M., Booth, J., Agusti, S., Saderne, V., Anton, A., Daffonchio, D., & Fusi, M. (2019) Oxygen supersaturation protects coastal marine fauna from ocean warming. *Science Advances*, **5**, eaax1814.

Gollock, M.J., Currie, S., Petersen, L.H., & Gamperl, A.K. (2006) Cardiovascular and haematological responses of Atlantic cod (Gadus morhua) to acute temperature increase. *Journal of Experimental Biology*, **209**, 2961–2970.

Grans, A., Jutfelt, F., Sandblom, E., Jonsson, E., Wiklander, K., Seth, H., Olsson, C., Dupont, S., Ortega-Martinez, O., Einarsdottir, I., Bjornsson, B.T., Sundell, K., & Axelsson, M. (2014)

Aerobic scope fails to explain the detrimental effects on growth resulting from warming and elevated CO2 in Atlantic halibut. *Journal of Experimental Biology*, **217**, 711–717.

Hunt, R.F., Hortopan, G.A., Gillespie, A., & Baraban, S.C. (2012) A novel zebrafish model of hyperthermia-induced seizures reveals a role for TRPV4 channels and NMDA-type glutamate receptors. *Experimental Neurology*, **237**, 199–206.

Jørgensen, L.B., Robertson, R.M., & Overgaard, J. (2020) Neural dysfunction correlates with heat coma and CT_{max} in *Drosophila* but does not set the boundaries for heat stress survival. *J Exp Biol*, **223**, jeb218750.

Jutfelt, F., Gräns, A., Jönsson, E., Wiklander, K., Seth, H., Olsson, C., Dupont, S., Ortega-Martinez, O., Sundell, K., Axelsson, M., & Sandblom, E. (2014) Response to 'How and how not to investigate the oxygen and capacity limitation of thermal tolerance (OCLTT) and aerobic scope – remarks on the article by Gräns et al.' *Journal of Experimental Biology*, **217**, 4433–4435.

Jutfelt, F., Norin, T., Ern, R., Overgaard, J., Wang, T., McKenzie, D.J., Lefevre, S., Nilsson, G.E., Metcalfe, N.B., Hickey, A.J.R., Brijs, J., Speers-Roesch, B., Roche, D.G., Gamperl, A.K., Raby, G.D., Morgan, R., Esbaugh, A.J., Gräns, A., Axelsson, M., Ekström, A., Sandblom, E., Binning, S.A., Hicks, J.W., Seebacher, F., Jørgensen, C., Killen, S.S., Schulte, P.M., & Clark, T.D. (2018) Oxygen- and capacity-limited thermal tolerance: blurring ecology and physiology. *Journal of Experimental Biology*, **221**.

Jutfelt, F., Roche, D.G., Clark, T.D., Norin, T., Binning, S.A., Speers-Roesch, B., Amcoff, M., Morgan, R., Andreassen, A.H., & Sundin, J. (2019) Brain cooling marginally increases acute upper thermal tolerance in Atlantic cod. *Journal of Experimental Biology*, **222**.

le Feber, J., Tzafi Pavlidou, S., Erkamp, N., van Putten, M.J.A.M., & Hofmeijer, J. (2016) Progression of Neuronal Damage in an In Vitro Model of the Ischemic Penumbra. *PLOS ONE*, **11**, e0147231.

Lefevre, S. (2016) Are global warming and ocean acidification conspiring against marine ectotherms? A meta-analysis of the respiratory effects of elevated temperature, high CO2 and their interaction. *Conserv Physiol*, **4**.

Lister, J.A., Robertson, C.P., Lepage, T., Johnson, S.L., & Raible, D.W. (1999) nacre encodes a zebrafish microphthalmia-related protein that regulates neural-crest-derived pigment cell fate. *Development*, **126**, 3757–3767.

Liu, J. & Baraban, S.C. (2019) Network Properties Revealed during Multi-Scale Calcium Imaging of Seizure Activity in Zebrafish. *eneuro*, **6**, ENEURO.0041-19.2019.

Lutterschmidt, W.I. & Hutchison, V.H. (2011) The critical thermal maximum: history and critique. *Canadian Journal of Zoology*,.

Marder, E., Haddad, S.A., Goeritz, M.L., Rosenbaum, P., & Kispersky, T. (2015) How can motor systems retain performance over a wide temperature range? Lessons from the crustacean stomatogastric nervous system. *J Comp Physiol A*, **201**, 851–856.

McArley, T.J., Hickey, A.J.R., & Herbert, N.A. (2018) Hyperoxia increases maximum oxygen consumption and aerobic scope of intertidal fish facing acutely high temperatures. *The Journal of Experimental Biology*, **221**, jeb189993.

McArley, T.J., Sandblom, E., & Herbert, N.A. (2020) Fish and hyperoxia—From cardiorespiratory and biochemical adjustments to aquaculture and ecophysiology implications. *Fish and Fisheries*,.

Morgan, R., Finnøen, M.H., & Jutfelt, F. (2018) CTmax is repeatable and doesn't reduce growth in zebrafish. *Scientific Reports*, **8**, 7099.

Moyano, M., Candebat, C., Ruhbaum, Y., Álvarez-Fernández, S., Claireaux, G., Zambonino-Infante, J.-L., & Peck, M.A. (2017) Effects of warming rate, acclimation temperature and ontogeny on the critical thermal maximum of temperate marine fish larvae. *PLOS ONE*, **12**, e0179928.

Muto, A., Lal, P., Ailani, D., Abe, G., Itoh, M., & Kawakami, K. (2017) Activation of the hypothalamic feeding centre upon visual prey detection. *Nature Communications*, **8**.

Overgaard, J., Andersen, J.L., Findsen, A., Pedersen, P.B.M., Hansen, K., Ozolina, K., & Wang, T. (2012) Aerobic scope and cardiovascular oxygen transport is not compromised at high temperatures in the toad Rhinella marina. *Journal of Experimental Biology*, **215**, 3519–3526.

Perry, A.L., Low, P.J., Ellis, J.R., & Reynolds, J.D. (2005) Climate Change and Distribution Shifts in Marine Fishes. *Science*, **308**, 1912–1915.

809 Pinsky, M.L., Eikeset, A.M., McCauley, D.J., Payne, J.L., & Sunday, J.M. (2019) Greater vulnerability
810 to warming of marine versus terrestrial ectotherms. *Nature*, **569**, 108–111.
811 Pörtner, H.O. (2002) Climate variations and the physiological basis of temperature dependent
812 biogeography: systemic to molecular hierarchy of thermal tolerance in animals. *Comparative*
813 *Biochemistry and Physiology Part A: Molecular & Integrative Physiology*, **132**, 739–761.
814 Pörtner, H.-O., Bock, C., & Mark, F.C. (2017) Oxygen- and capacity-limited thermal tolerance:
815 bridging ecology and physiology. *J Exp Biol*, **220**, 2685–2696.
816 Pörtner, H.O. & Knust, R. (2007) Climate Change Affects Marine Fishes Through the Oxygen
817 Limitation of Thermal Tolerance. *Science*, **315**, 95–97.
818 R Core Team (2020) *R: A Language and Environment for Statistical Computing*. R Foundation for
819 Statistical Computing, Vienna, Austria.
820 Robertson, R.M. & Money, T.G. (2012) Temperature and neuronal circuit function: compensation,
821 tuning and tolerance. *Current Opinion in Neurobiology*, **22**, 724–734.
822 Sawant-Pokam, P.M., Suryavanshi, P., Mendez, J.M., Dudek, F.E., & Brennan, K.C. (2016)
823 Mechanisms of Neuronal Silencing After Cortical Spreading Depression. *Cerebral Cortex*, **27**.
824 Schindelin, J., Arganda-Carreras, I., Frise, E., Kaynig, V., Longair, M., Pietzsch, T., Preibisch, S.,
825 Rueden, C., Saalfeld, S., Schmid, B., Tinevez, J.-Y., White, D.J., Hartenstein, V., Eliceiri, K.,
826 Tomancak, P., & Cardona, A. (2012) Fiji: an open-source platform for biological-image
827 analysis. *Nature Methods*, **9**, 676–682.
828 Schulte, P.M. (2015) The effects of temperature on aerobic metabolism: towards a mechanistic
829 understanding of the responses of ectotherms to a changing environment. *Journal of*
830 *Experimental Biology*, **218**, 1856–1866.
831 Seneviratne, S.I., Donat, M.G., Mueller, B., & Alexander, L.V. (2014) No pause in the increase of hot
832 temperature extremes. *Nature Climate Change*, **4**, 161–163.
833 Sherman, E. & Levitis, D. (2003) Heat hardening as a function of developmental stage in larval and
834 juvenile Bufo americanus and Xenopus laevis. *Journal of Thermal Biology*, **28**, 373–380.
835 Shinnar, S. & Glauser, T.A. (2002) Febrile Seizures. *J Child Neurol*, **17**, S44–S52.
836 Spong, K.E., Andrew, R.D., & Robertson, R.M. (2016) Mechanisms of spreading depolarization in
837 vertebrate and insect central nervous systems. *J Neurophysiol*, **116**, 1117–1127.
838 Stillman, J.H. (2019) Heat Waves, the New Normal: Summertime Temperature Extremes Will Impact
839 Animals, Ecosystems, and Human Communities. *Physiology*, **34**, 86–100.
840 Sunday, J.M., Bates, A.E., & Dulvy, N.K. (2012) Thermal tolerance and the global redistribution of
841 animals. *Nature Climate Change*, **2**, 686–690.
842 Tang, L.S., Taylor, A.L., Rinberg, A., & Marder, E. (2012) Robustness of a Rhythmic Circuit to Short-
843 and Long-Term Temperature Changes. *Journal of Neuroscience*, **32**, 10075–10085.
844 Verberk, W.C.E.P., Leuven, R.S.E.W., Velde, G., & Gabel, F. (2018) Thermal limits in native and alien
845 freshwater peracarid Crustacea: The role of habitat use and oxygen limitation. *Functional*
846 *Ecology*, **32**, 926–936.
847 Verberk, W.C.E.P., Overgaard, J., Ern, R., Bayley, M., Wang, T., Boardman, L., & Terblanche, J.S.
848 (2016) Does oxygen limit thermal tolerance in arthropods? A critical review of current
849 evidence. *Comparative Biochemistry and Physiology Part A: Molecular & Integrative*
850 *Physiology*, **192**, 64–78.
851 Vladimirov, N., Mu, Y., Kawashima, T., Bennett, D.V., Yang, C.-T., Looger, L.L., Keller, P.J.,
852 Freeman, J., & Ahrens, M.B. (2014) Light-sheet functional imaging in fictively behaving
853 zebrafish. *Nature Methods*, **11**, 883–884.
854 Wang, T., Lefevre, S., Iversen, N.K., Findorf, I., Buchanan, R., & McKenzie, D.J. (2014) Anaemia only
855 causes a small reduction in the upper critical temperature of sea bass: is oxygen delivery the
856 limiting factor for tolerance of acute warming in fishes? *Journal of Experimental Biology*, **217**,
857 4275–4278.
858 Wenzel, M., Hamm, J.P., Peterka, D.S., & Yuste, R. (2017) Reliable and Elastic Propagation of Cortical
859 Seizures In Vivo. *Cell Reports*, **19**, 2681–2693.
860 Woitzik, J., Hecht, N., Pinczolits, A., Sandow, N., Major, S., Winkler, M.K.L., Weber-Carstens, S.,
861 Dohmen, C., Graf, R., Strong, A.J., Dreier, J.P., Vajkoczy, P., & For the COSBID study group
862 (2013) Propagation of cortical spreading depolarization in the human cortex after malignant
863 stroke. *Neurology*, **80**, 1095–1102.